EFDA
EUROPEAN FUSION DEVELOPMENT AGREEMENT

Istituto di Fisica del Plasma "Piero Caldirola"
Consiglio Nazionale delle Ricerche

CONSIGLIO NAZIONALE DELLE RICERCHE

Study of scavenging effect to reduce the redeposition of hydrogenated coatings containing carbon and tungsten (EFDA Task-WP10-PWI-02-02-01BS)

Espedito Vassallo[1], Maurizio Canetti[2], Anna Cremona[1], Fabio Dell'Era[1], David Dellasega[3], Francesco Ghezzi[1], Giovanni Grosso[1], Laura Laguardia[1], Matteo Passoni[3],

[1]CNR, Istituto di Fisica del Plasma "P.Caldirola", Italy
[2]CNR, Istituto per lo Studio delle Macromolecole, Italy
[3]Politecnico di Milano, Dipartimento di Energia, Italy

FP 11/2 March, 2011

ISTITUTO DI FISICA DEL PLASMA
"Piero Caldirola"

Associazione EURATOM-ENEA-CNR

Via R. Cozzi 53 - 20125 Milano (Italy)

Introduction

Carbon and tungsten sputtering in the top surface of the divertor with subsequent redeposition in the inner and sub-divertor area of amorphous carbon (a-C/W:T) films is a major concern for the operation of ITER because it will contribute significantly to tritium retention. The injection of scavenger particles in divertor plasmas has been proposed as a possible technique to inhibit the formation of tritium-rich carbon films during normal plasma operation. The phenomenon of the scavenging effect to reduce the redeposition of amorphous hydrogenated carbon (a-C:H) films has been largely investigated and good results have been obtained [1]. The knowledge about codeposition of carbon and tungsten with hydrogen isotopes needs to be developed. In this specific theme, IFP has obtained a task-EFDA-WP10-PWI-02-02-01/BS. In this task, the scavenging effect to reduce the redeposition of hydrogenated films containing carbon and tungsten was studied. Experiments in low temperature laboratory plasmas driven with radio frequency were executed. The role of the interaction of nitrogen mixtures plasmas during the growth of amorphous carbon (a-C/W:H) films was analysed. The effect of temperature was also investigated. Mass spectrometry was used to characterize the gas composition during the process. The deposition rates were measured by a surface profiler. The surface chemical characterization was carried out by means of X-ray photoelectron spectroscopy (XPS). The structural properties were studied by X-ray diffraction measurements (XRD) and by atomic force microscopy (AFM).

2. Experimental set-up

2.1. The plasma reactor

Experiments were performed by an RF plasma sputtering system already described [2]. In order to reproduce a co-deposited film of a tokamak as a “reference sample”, hydrogenated a-C/CW coatings were deposited on (100) oriented silicon wafers using a pure tungsten target, which works as RF electrode, in an Ar/CH_4 (50 sccm:1 sccm) gas mixture. In order to study the scavenging effect, nitrogen was injected in Ar/CH_4 plasma with gas flow rates in the range of 1-20 sccm. The wafers were placed on the ground electrode at 6.5 cm away from the target and a heating system was supplied to the electrode. The overall sputtering pressure, measured by a capacitive vacuum gauge, was fixed at 3 Pa ($n \cong 10^{21}$ m^{-3}). High-purity (99.9997%) argon, methane and nitrogen gases were injected into the plasma region through a loop nozzle between the target and the grounded electrode. The process pressure was monitored to be constant admitting fixed gas flow rates via mass flow controllers, and pumping the processed gas by a turbomolecular pump. The RF power was fixed at 200 W and the DC self-bias sputtering voltage established in the reactor was 1150 V.

2.2. Instrument set-up

The plasma phase was investigated by optical emission spectroscopy (OES) through a quartz window. The optical collection axis was centred on the bulk of the plasma discharge at 90° from the interelectrode axis, i.e. parallel to the electrodes surface. The experimental apparatus consists of a scanning monochromator (Horiba Jobin Yvon iHR550) of the Czerny-Turner type, with a focal length of 0.55 m, built around a holographic diffraction grating with 1800 grooves mm^{-1}, coupled with a CCD (Synapse Horiba Jobin Yvon) camera, thermoelectrically cooled to −70 °C. Spatially averaged (≈1 cm^3) plasma emission was collected with a plane-convex convergent lens of 1 inch diameter and focused through an optical fibre (length 3m, core 600μm, numerical aperture 0.22) onto the entrance slit of the monochromator, kept at 50μm. Coloured glass filters were used to remove higher diffraction orders from the light. The spectra were acquired in the wavelength range 300-1000 nm with an integration time of 5 s. The spectral resolution of this system is 0.06 nm. An RF quadrupole mass spectrometer (Balzers PRISMA QMS200) with mass resolution 1, connected to the vessel with a differentially pumped chamber ($P_0 = 5 \times 10^{-7}$ mbar), was used to characterize the residual gas composition during the process. The deposition rates were measured by a P15 surface profiler (KLATencor San Jose, CA). The surface chemical characterization was carried out by means of X-ray photoelectron spectroscopy (XPS). The core level spectra have been acquired using a nonmonochromatized Al anode X-ray source ($h\nu$ =1486.6 eV) VSW model TA10 and a hemispherical analyzer VSW model CLASS 100, equipped with a single channel detector, operating in constant pass Energy mode (22 eV) with 0.9 eV of overall resolution. The structural properties studied by X-ray diffraction measurements were performed with a wide angle Siemens D-500 diffractometer (WAXD) equipped with a Siemens FK 60-10 2000W tube in grazing incidence geometry. The radiation was a monochromatized Cu Kα beam with wavelength λ = 0.154056 nm. The operating voltage and current were 40 kV and 40 mA, respectively. The data were collected in the 1-4.2° range of 2θ angles with a step of 0.01° by means of a silicon multi-cathode detector

Vortex-EX (SII). The morphological properties were investigated by atomic force microscopy (AFM) and scanning electron microscopy (SEM). AFM measurements were made in air by a Nano-RTM AFM System (Pacific Nanotechnology, Santa Clara, CA, USA) operating in close-contact mode. Silicon conical tips of 10 nm radius mounted on silicon cantilevers of 125 mm length, 42 N/m force constant and 320 KHz resonance frequency were used. Images were processed and analyzed by means of the NanoRule+^{TM} software provided by Pacific Nanotechnology. SEM measurements were made by ZEISS Supra 40 System equipped with *in lens* detector using an accelerating voltage of 15 kV. Elemental analisys (EDS) was performed using an INCA detector from Oxford Instruments.

3. Results and discussion

3.1 Reference sample preparation

Hydrogenated a-C/CW coatings were deposited in an Ar/CH_4 (50:1) plasma. The deposition was performed for 60 min. The deposition rate, estimated from the measurement of the film thickness was found to be about 4 nm/min.

3.1.1 Chemical bonding states

The chemical composition of a-C/CW coatings in atomic % was deduced by XPS analysis. The analysis showed a composition richer in carbon than in tungsten. Due to the air exposure during the transfer of the samples from the reactor chamber to the XPS device an oxygen uptake was observed. The oxide layers were removed by Ar sputtering at 3.0 keV and 0.5μA of sample current for 30 min in order to not deteriorate the structure of the film itself. The choice of these parameters was based on previous experience. Using the atomic sensitivity factors given in literature, the relative atomic concentrations have been calculated from the areas under the peaks. The C/W ratio of the atomic concentrations varied form 5.2 to 2.8 before and after Ar sputtering. The survey spectrum showed the presence of W, C and O only. The chemical state of W and C was studied by fitting the high resolution spectra of the respective core level lines. W was found to be predominantly in the WO_3 phase before the sputtering. Instead after the sputtering the predominant species was a non stoichiometric tungsten carbide so that the reference sample could be taken as representative of a deposited film in a tokamak.

An example of W*4f* core level XPS spectrum for a-C/CW:H coating, after Ar sputtering, is shown in fig. 1. The spectrum exhibit the spin-orbit split of $4f_{7/2}$ and $4f_{5/2}$ components of the W4f core levels, separated by about 2.1 eV.

Data reported in the literature assign the W $4f_{7/2}$ binding energy for metallic tungsten at 31.4 eV and the stoichiometric WC at 32.2 eV[6]. Pauleau and Gouy-Pailler[7] found for the WC_{1-x} phase a value of 31.9 eV. This value is also characteristic[8] of WC/a-C coatings with carbon concentration above 40 at.%. According with ref 7, the component at BE 32.03 eV is assigned to a WC_{1-x} phase while the component at BE 31.44 eV is assigned to metallic tungsten. Last, the component at BE 35.47 eV is assigned to WO_3 residual oxide. The WC_{1-x} phase assignment is supported by XRD analysis (fig. 6), as it will be explained in Sec. 3.1.3.

The fitting of the C1s level, presented in figure 2, corroborates this findings. Values for the tungsten carbide have been reported in literature in the 282.6-284.4 eV range[3, 4-5]. The lower values in this range correspond to stoichiometric WC, while the higher values are more predominant when non stoichiometric tungsten carbide is deposited. Using the findings of ref 3, 4

and 5 the component at BE 283.6 eV is assigned to the non stoichiometric tungsten carbide (WC_{1-x} phase), the component at 285 eV to hydrogenated amorphous carbon and the last component at BE 286.8 eV to C-O binding type.

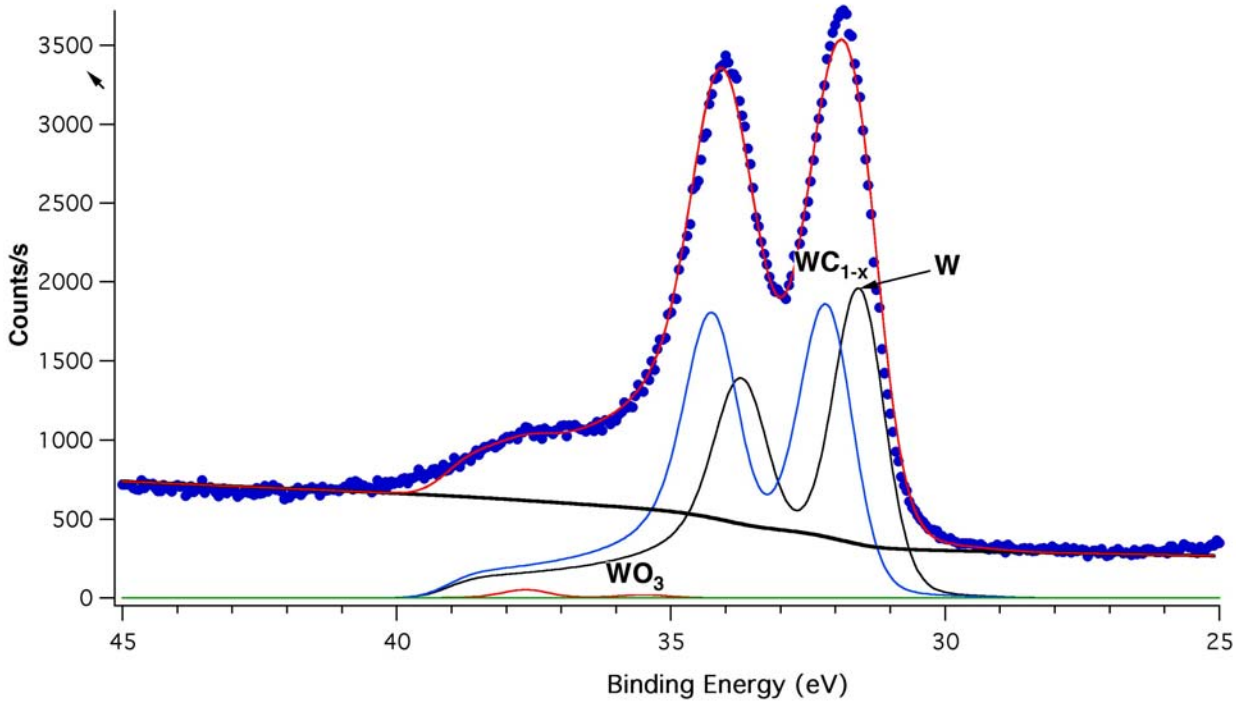

FIG. 1. High resolution XPS spectrum for the W4 *f* core level after sputtering.

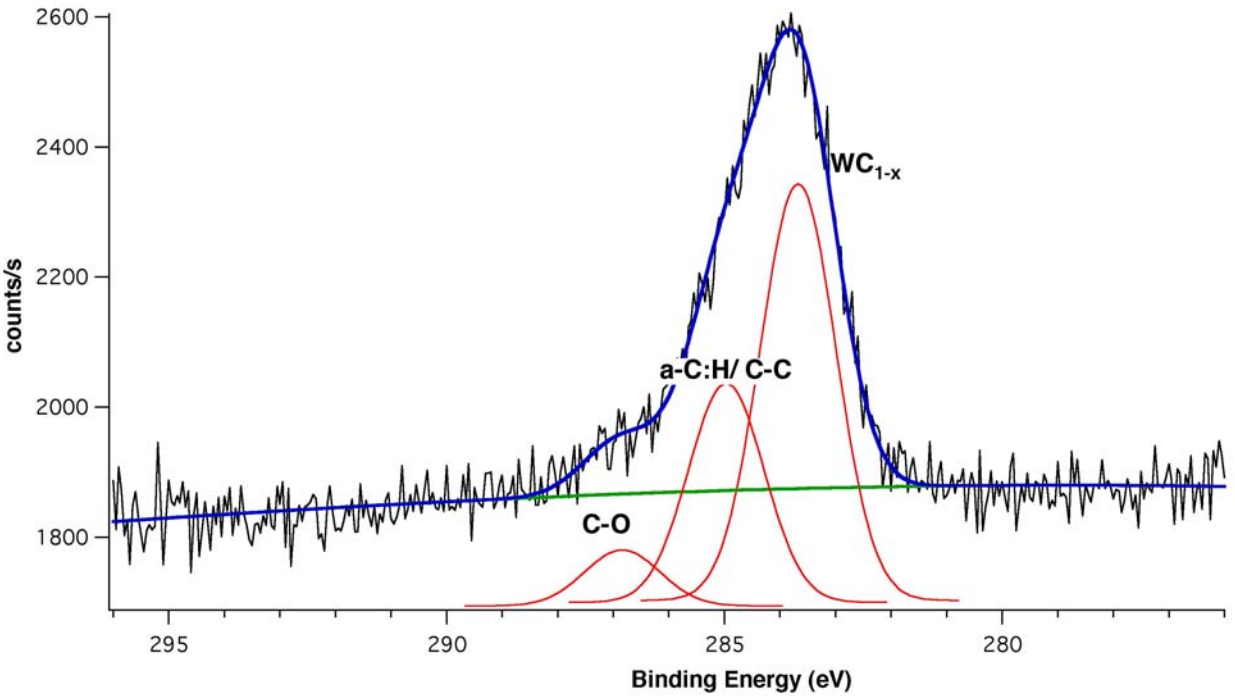

FIG. 2. High resolution XPS spectrum for the C1*s* core level after sputtering.

3.1.2 Surface morfology

The reference sample (a-C/CW) was analyzed by SEM analysis. Fig. 3 shows that the coating is rather uniform and consists of globules with average diameters <100 nm. The coating consisted of C, W and O as confirmed by Energy Dispersive Spectrometry (EDS) analysis, see Fig. 4.

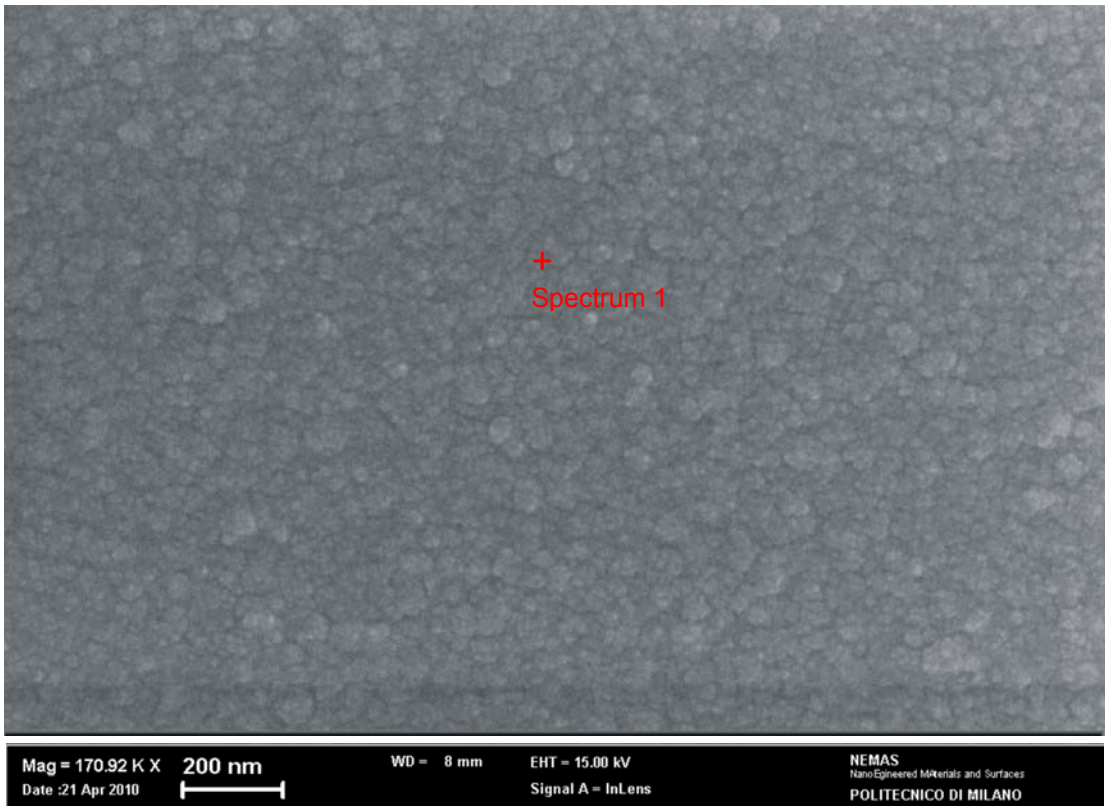

Fig. 3. SEM image of as-deposited a-C/CW coating

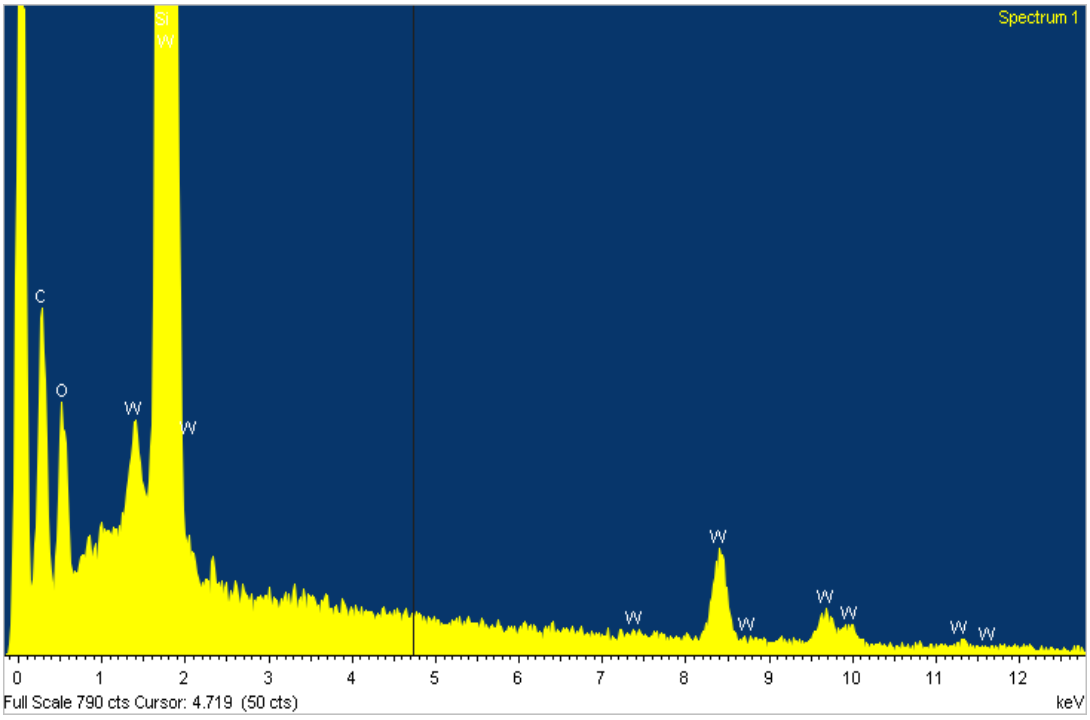

Fig. 4. EDS of marked region of Fig. 2.

The coating morphology of the reference sample is evident also in AFM picture. The analysis shows that the surface morphology is rather flat, characterized by uniformly distributed globules, with roughness R_{rms} of 2.45 nm on an area of 4.83 μm^2.

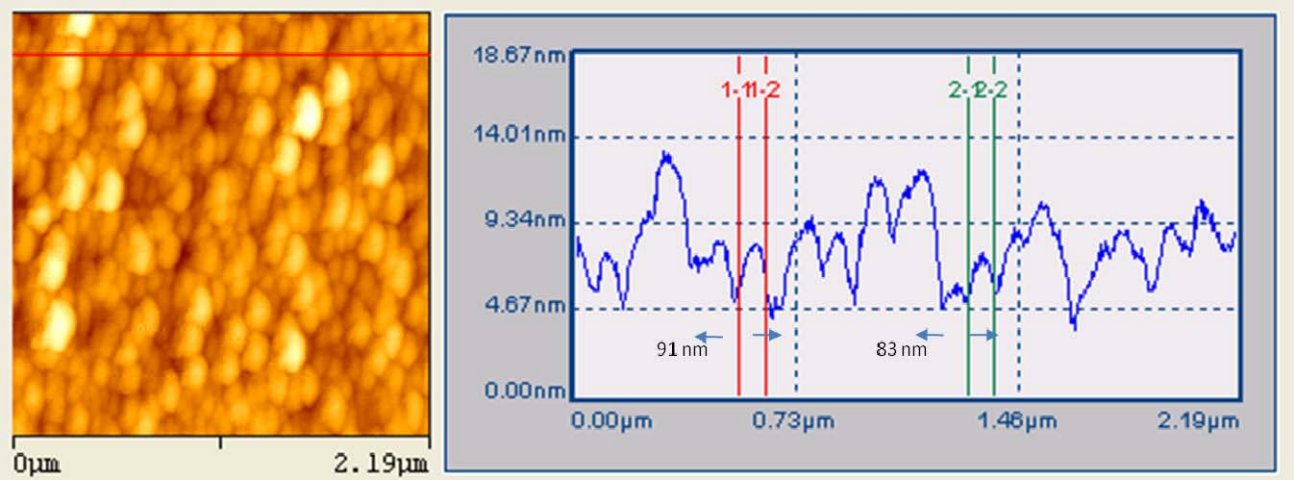

Fig. 5. AFM image of as-deposited a-C/CW coating

3.1.3 Coating structure

Figure 6 presents the diffractogram of as-deposited W-C coatings. The analysis reveals, besides the reflection at 69.3° 2θ corresponding to Si, a broad peak at 37° 2θ. The position of this peak is well matched[9-10] with a two components mixture of β-WC_{1-x} phase [(111) and (200) orientations].

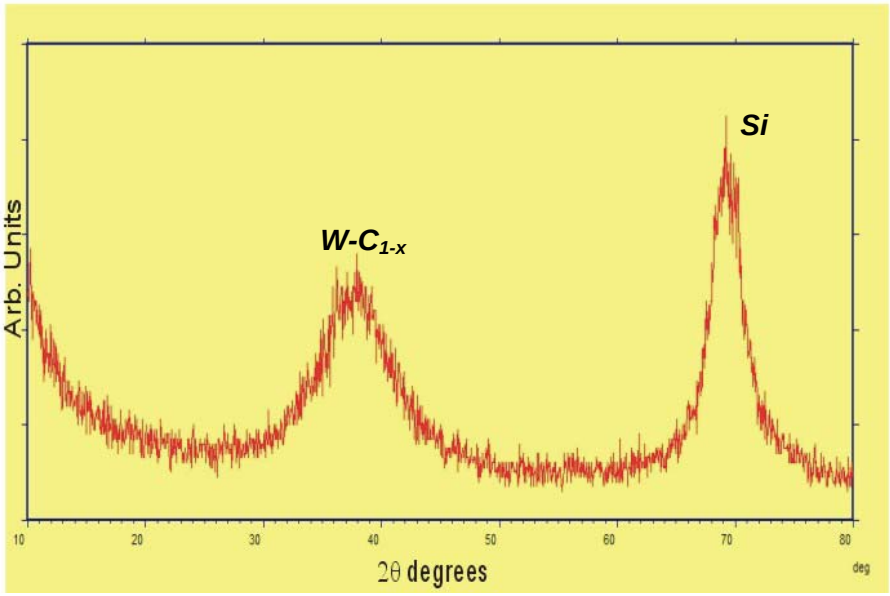

Fig. 6. XRD pattern of as-deposited a-C/CW coating

3.1.4 Analysis of plasma phase

Optical Emission Spectroscopy (OES) of the plasma phase during the growth of (a-C/W:H) coatings has revealed the presence of Ar, H and W neutral atoms, Ar ions (ArII) and CH radicals (Fig. 7-8). CH 4300-Å system ($A^2\Delta$ - $X^2\Pi$), H_2 Fulcher α- system ($d^3\Pi_u$ – $a^3\Sigma_g$) and neutral W lines have been monitored to control the process during the deposition of the reference sample.

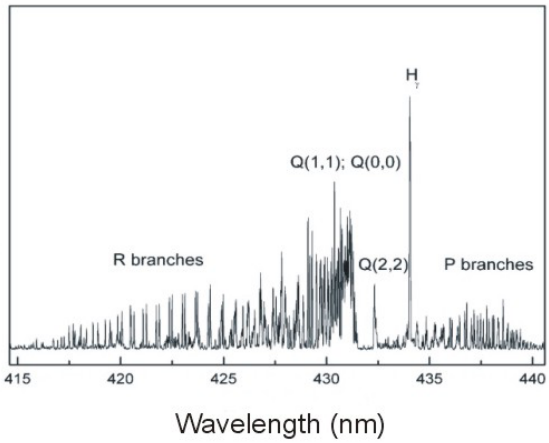

Figure 7. Emission spectrum in the 415-440 nm range (CH 4300-Å system).

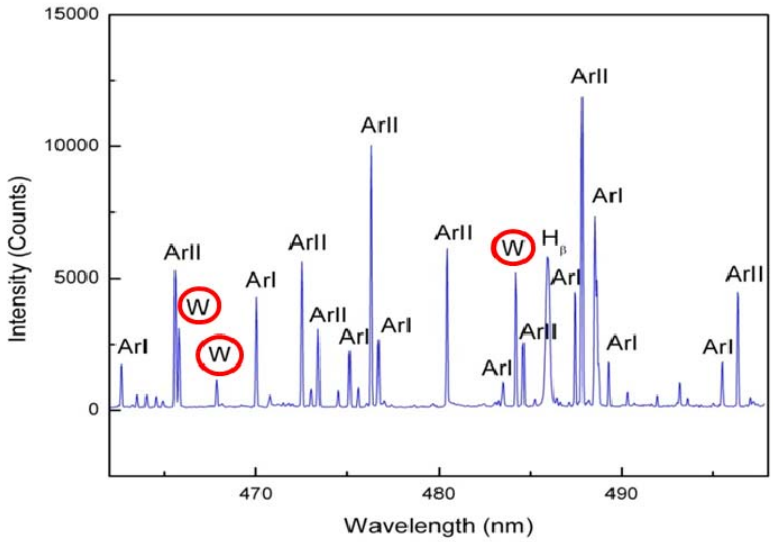

Figure 8. Emission spectrum in the 460-500 nm range.

CH 4300-Å and H_2 Fulcher α emission bands give information about the fragmentation of methane molecules. CH*(A) excited radicals are produced by electron dissociative excitation of methane molecules according to the following reactions :

$CH_4 + e \rightarrow CH^*(A) + H_2(X) + H + e$ $\quad E_{thr} = 12.1$ eV (1)

$CH_4 + e \rightarrow CH^*(A) + 3H + e$ $\quad E_{thr} = 16.6$ eV (2)

CH*(A) excited radicals could also be formed by electron impact dissociation of larger molecules (C_2H_2, $C_2H_2^+$, C_2H_4) but the required energy is higher than 23 eV. Because the plasma temperature is of the order of few eV, this channel can be ignored. Moreover electron impact excitation of CH ground state radicals is not competitive because they react quickly with the background gas molecules and therefore their concentration in the discharge is very low.

Excited H_2^* ($d^3\Pi_u$) molecules are mainly produced in the methane plasma by direct electron impact dissociation of hydrogen molecules,

$$H_2 + e \rightarrow H_2^* (d^3\Pi_u) + e \qquad E_{thr} = 13.84 \text{ eV} \qquad (3)$$

because electron dissociative excitation of methane molecules needs a threshold energy 23.24 eV:

$$CH_4 + e \rightarrow CH_2 + H_2^*(d^3\Pi_u) + e \qquad E_{thr} = 23.24 \text{ eV} \qquad (4)$$

Excited levels of $CH^*(A^2\Delta)$ radicals and H_2^* ($d^3\Pi_u$) molecules are depopulated via spontaneous emission because their lifetimes are $\tau = 5 \times 10^{-7}$ s and $\tau = 6.3 \times 10^{-8}$ s respectively, whereas their collision frequency with methane molecules is of the order 10^4-10^5 s^{-1}, that is the radiative decay prevails over its quenching in collisions with methane molecules. W excited states are populated via electron impact and their radiative de-excitation gives information about the physical sputtering of the W target.

3.2 Minimization of a-C/W:H coatings growth

The study of scavenging effect was tested by the injection of nitrogen in Ar/CH_4 (50 sccm: 1 sccm) plasma. The nitrogen flow was varied between 1-20 sccm.

3.2.1 Analysis of plasma phase

The analysis of the plasma phase during the growth of (a-C/W:H) coating with the nitrogen dilution is shown in figure 9. The CH 4300-Å system, the atomic hydrogen lines H_γ (434.05 nm), H_δ (410.17 nm), the N_2 second positive system ($C^3\Pi_u$-$B\Pi_g$), the N_2^+ first negative system ($B^2\Sigma_u$+-$X^2\Sigma_g^+$) and the CN violet system ($B^2\Sigma^+$-$X^2\Sigma^+$) have been observed. To interpret the optical emission relative to the CN violet system, different kinetic mechanisms have been supposed[12-13]:

$$N + CH_2 \rightarrow CN + H_2 \qquad (5)$$

$$N + CH_2 \rightarrow CN + H + H \qquad (6)$$

$$C + N_2 \rightarrow CN + N \qquad (7)$$

$$CH_x^* + N_2^* \rightarrow CN + N + H_y + H_z + e \qquad (x = y + z) \qquad (8)$$

$$N + CH \rightarrow CN(B) + H \qquad (9)$$

$$C + N + N_2 \rightarrow CN(B) + N_2 \qquad (10)$$

The first four chemical reactions lead to the formation of ground state CN molecules which will be excited by electron impact. The other two chemical reactions lead directly to the formation of excited CN molecules. A further possible route leading to the formation of ground state CN molecules involves the initial formation of a stable intermediate compound containing C-N bonding which then yields CN on further reactions with active plasma species A:

$$CH_x^* + N_2^* \rightarrow CNH_y + N + H_z + e \qquad (x = y + z) \qquad (11)$$

$$CNH_y + A^* \rightarrow CN + A + H_z + H_\alpha + e \qquad (y = z + \alpha) \qquad (12)$$

Because OES has not revealed atomic carbon, and this consistent with the high threshold energy for its production from methane molecules, we suppose the channels (7) and (10) negligible.

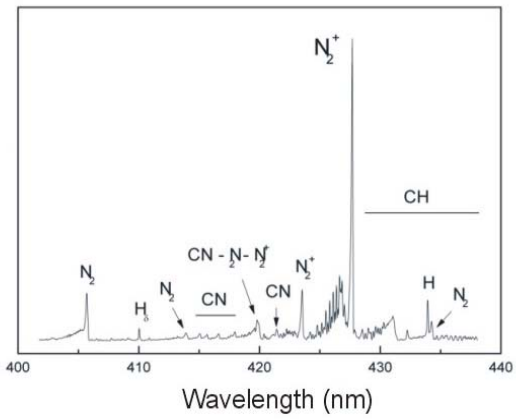

Figure 9. Emission spectrum of the $Ar/CH_4/N_2$ plasma in the 400-440 nm range.

The dilution of the Ar/CH_4 plasma in nitrogen does not change the self-bias potential, which remains nearly constant at around 1150 V, and as a consequence does not change the energy of the ions but only the plasma chemical composition. The nitrogen addition produces various species deriving from N_2, while the peaks associated with hydrocarbon species slightly decrease. In particular, CN emission groups appear. Figure 10 shows CN and CH band intensities as a function of the nitrogen dilution.

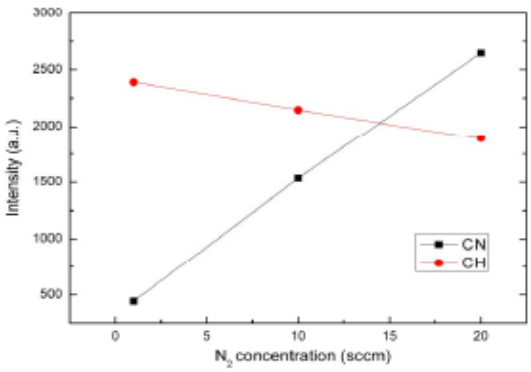

Figure 10. Trend of CH and CN radicals as a function of nitrogen dilution.

The deposition rate of a-C/W:H coating, given in figure 11 as a function of nitrogen dilution, strongly decreases up to a nitrogen flux of 10 sccm. As expected, an incomplete suppression of the deposition was found, contrary to the case of a-C:H films growth[1]. In our case two factors could explain this effect. The former is the low chemical reactivity of W in the plasma phase to form volatile compounds and the latter is the low chemical sputtering yield of W containing coatings. This rationale is supported by the observation of W-N bounds by XPS analysis (Fig. 12). Looking at Fig 11, beyond 10 sccm of nitrogen flux a gradual rise in the deposition rate was noted. This effect has not been yet investigated. At the present, our opinion is that increasing the nitrogen flow above 10 sccm all the chemical reactions with nitrogen are shifted toward the solid phase with production of tungsten nitride.

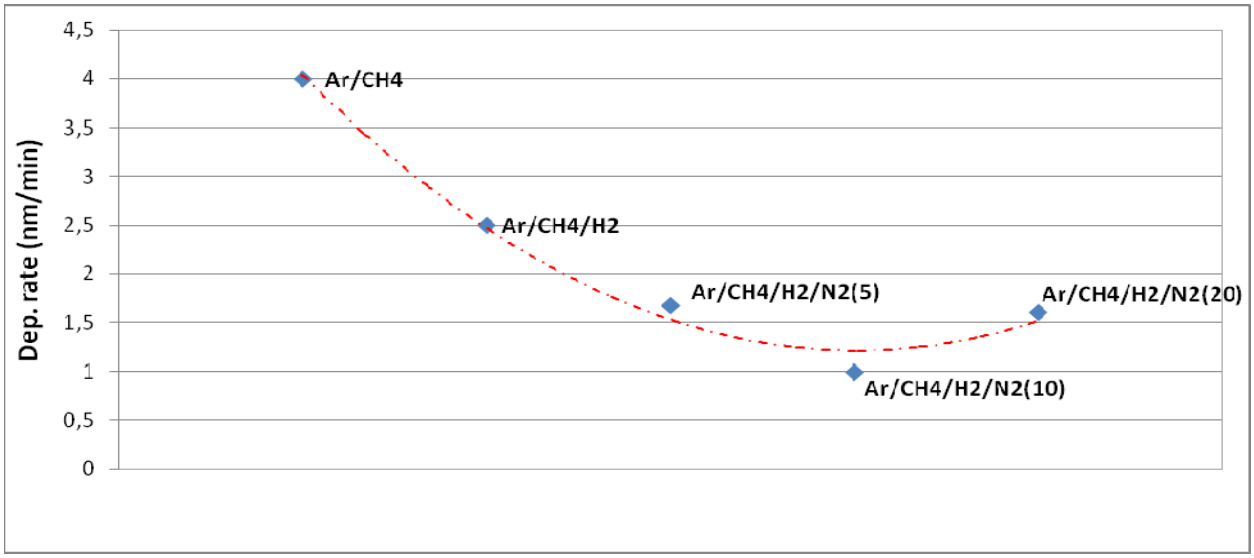

Figure 11. Evolution of the deposition rate in Ar/CH_4 plasma as a function of nitrogen dilution, 5,10, 20 cm^3 min^{-1} (rf power=200 W, Vbias= 1150 V, Pressure=3 Pa)

3.2.2 Carbon content

Besides the reduction of the coatings growth, a further positive result leading to a minimization of tritium retention is the decrease of carbon content in the coating produced with the nitrogen flow (Fig. 12). The C/W ratio was found to decrease from 2.8 to 0.5 increasing the nitrogen flow up to 5 sccm. Above this value there are no further improvements**.**

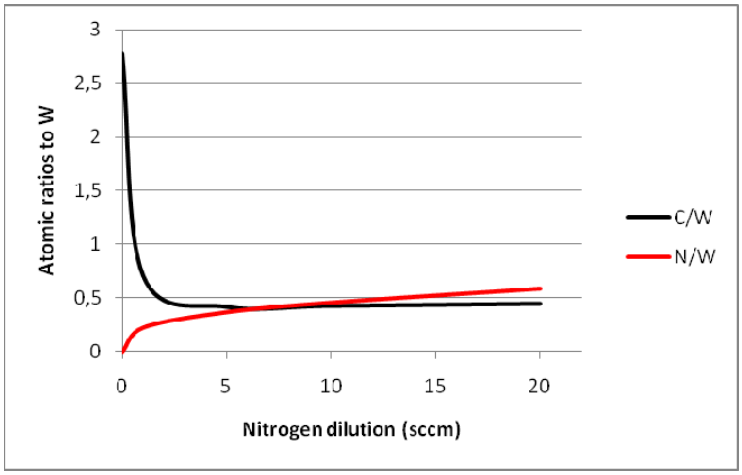

Figure 12. Evolution of the C/W and N/W ratio as a function of nitrogen dilution evaluated by XPS.

3.2.3 Mass spectrometry analysis

A common problem for RF quadrupole is the mass peak assignment due to the possible contribution by different species. Before working with the plasma, the mass assignment was carried out by admitting flow mixtures as Ar/CH_4/H_2/N_2 and Ar/CH_4/H_2 and with the help the NIST database [14]. In this way it was possible to assign *m/e*= 27 to the HCN species, *m/e*= 28 to C_2H_4 and N_2, *m/e*= 16 to CH_4, *m/e*= 41 to CH_3CN and *m/e*= 59 to C_3H_9N. Switching on the plasma no further radicals in the gas phase were created in these specific cases. This allowed us to observe the change in the amount of volatile species introducing nitrogen in the plasma looking only at the above m/e values. Fig. 13 shows a comparison between the two mixtures for the case of nitrogen

flow at 20 sccm. Notice the strong increase of volatile molecules as HCN and C_2H_4 (*m/e*= 28) with the nitrogen injection. A light increase of minor volatile products as C_2H_2, CH_3CN and C_3H_9N has also been detected. To explain the increase of *m/e*= 16 and 28 one has to invoke all the possible recombination reactions, even though this aspect is out of our purpose.

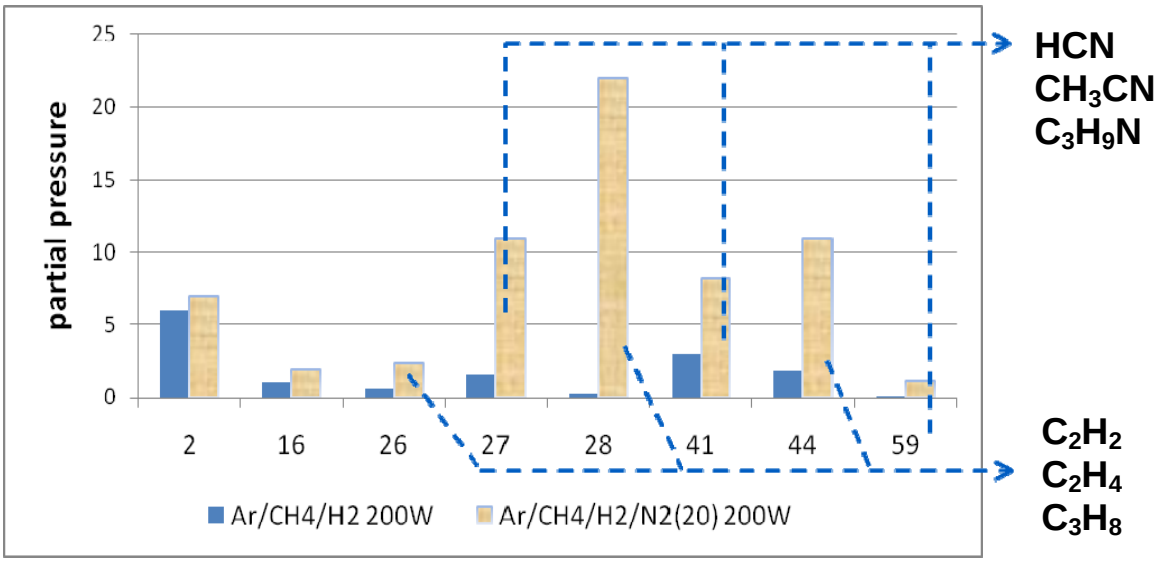

Figure 13. Mass spectra of Ar/CH4/H2 (50:1:1) and Ar/CH4/H2/N2 (50:1:1:20) plasmas at 3 Pa. Partial pressure units: for amu 2, 16, 28 ($x10^{-6}$mbar), for amu 26, 27, 41, 44, 59 ($x10^{-7}$ mbar)

3.3 Discussion

The decrease of the a-C/WC:H coatings growth can be mainly explained by the fast reactions in plasma phase by the precursors, like radical CH_3, CH_2, CH with nitrogen and hydrogen to form and increase the above volatile species as revealed by the mass spectrometry (fig13).

Obviously, the nitrogenated and hydrocarbon volatile molecules could also form by the hydrogen abstraction of deposited coating during the plasma-surface interaction. In order to analyse the hydrogen effect as an etching element, a hydrogenated a-C/CW coating (thickness ≈ 400 nm) was exposed to the Ar/CH_4/H_2/N_2(10) plasma experiment. No etching rate was found, on the contrary a deposition was found (≈ 1 nm/min). This result demonstrates that at the plasma-surface interface there could be an equilibrium between incoming and outgoing species by the abstraction of hydrogen atoms, but this process is not preponderant in comparison with the gas phase reactions in plasma. Regarding the surface effects on the sample holder electrode, since the value of the voltage drop was about -10V and the average energy of ions, due to the collisional motion within the sheath, was close to a few electronvolts, the ion bombardment was assumed to be negligible. At last, in all experiments at room temperature, since the temperature (≈ 300 K) of the electrode was not significantly changed when the power increased from 100 to 300 W, the temperature activated chemical erosion processes were assumed to be negligible.

In order to have further knowledge, the temperature dependance of the deposition of a-C/CW coatings was investigated. In Fig. 14 the deposition rate is plotted as a function of the substrate temperature in the range of 300-570 K. Because the rate shows no significant temperature dependence in this range, it may be speculated that the active processes are essentially temperature independent in the analysed range.

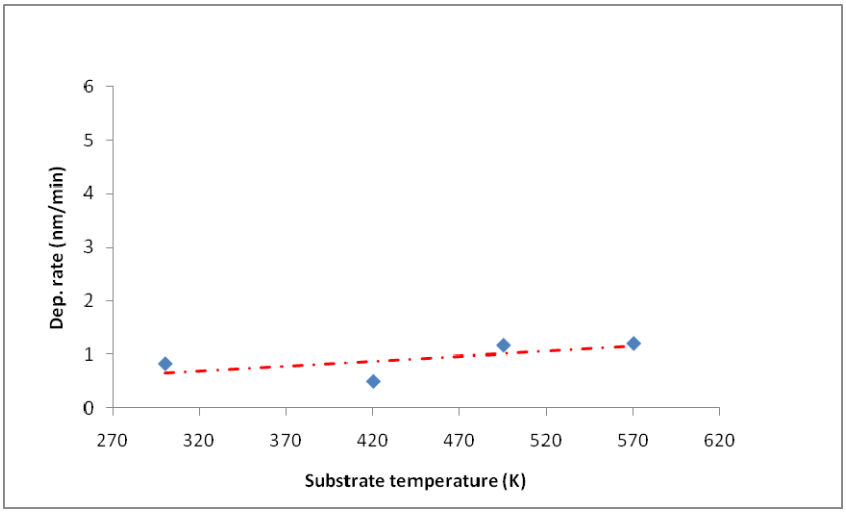

Figure 14. Evolution of the deposition rate in $Ar/CH_4/H_2/N_2(10)$ plasma as a function of the substrate temperature (rf power=200 W, Vbias= 1150 V, Presure=3 Pa)

Conclusions

The experimental results indicate that the minimization of tritium-rich C/W coatings in the divertor area by physical-chemical processes is a feasible goal. A strong decrease in the deposition rate of C/W coatings was found with a nitrogen flux of 10 sccm. Besides the minimization of the deposition, a decrease of carbon in the coating as a function of nitrogen dilution was found. This finding in fundamental in order to minimize the tritium retention correlated with the amount of carbon. However, further experiments should identify the suitable injection position and the minimum density of the scavenger gas as a function of hidden areas of the divertor.

References

[1] E Vassallo, S Barison, A Cremona, G Grosso, M Fabrizio and L Laguardia, Plasma Phys. Control. Fusion 52 (2010) 075014

[2] B. Despax and J. L. Flouttard, Thin Solid Films 168 (1989) 81-88

[3] R. J. Colton, J. W. Rabalais, Inorg. Chem., 15 (1976) 236

[4] J. F. Coulon, G. Turban, Mater. Sci. Eng. A, 139 (1991) 385

[5] P. K. Srivastava, V. D. Vankar, K. L. Chopra, J. Vac. Sci. Technol. A, 4 (1986) 2819

[6] J. F. Moulder, W. F. Stickle, P. E. Sobol, and K. D. Bomben, Handbook of X-ray Photoelectron Spectroscopy, edited by J. Chastain and R. C. King, Jr. (Physical Electronics, Eden Prairie, MN, 1995), pp. 216 and 241.

[7] Y. Pauleau and Ph. Gouy-Pailler, J. Mater. Res. **7**, 2070, 1992.

[8] A. A. Voevodin, J. P. O'Neill, S. V. Prasad, and J. S. Zabinski , J. Vac. Sci. Technol. A 17, N°3, May/Jun (1999) 986-992

[9] Kim, D.; Kim, O.H.; Anderson, T.J.; Koller, J.; McElwee-White, L.; Leu, L.C.; Tsai, J.M.; Norton, D.P., *J. Vac. Sci. Technol,* **2009**, *27*, 943-950

[10] Rincón C, Romero J, Esteve J, et al. , Surf Coat Technol, 2003, 163-164: 386—391

[11] R. H. Janev and D. Reiter, Phys. Plasmas 9, 4071 (2002)

[12] C.D. Pintassilgo, G. Cernogora, J. Loureiro, Plasma Sources Sci. Technol. 10 (2001) p. 147-161

[13] S. V. Avtaeva, T. M. Lapochkina, Plasma Physics Reports, 2007, Vol. 33, No. 9, p. 774-785

[14] Linstrom PJ, Mallard WG (Eds) NIST Chemistry Web-Book, NIST Standard Reference Database Number 69, March 2003, National Institute of Standards and Technology, Gaithersburg MD, 20899 (http://webbook.nist.gov).